Random magnetic anisotropy driven transitions in the layered perovskite $LaSrCoO_4$

Abdul Ahad,[1,*] K. Gautam,[2,†] S. S. Majid,[1,‡] K. Dey,[2] A. Tripathy,[2] F. Rahman,[1] R. J. Choudhary,[2] R. Sankar,[3] A. K. Sinha,[4,§] S. N. Kaul,[5,¶] and D. K. Shukla[2,‖]

[1]*Department of Physics, Aligarh Muslim University, Aligarh 202002, India*
[2]*UGC-DAE Consortium for Scientific Research, Indore 452001, India*
[3]*Institute of Physics, Academia Sinica, Taipei 11529, Taiwan*
[4]*Indus Synchrotrons Utilization Division, Raja Ramanna Center for Advanced Technology, Indore 452013, India*
[5]*School of Physics, University of Hyderabad, Hyderabad 500046, India*

(Received 19 February 2023; revised 16 April 2023; accepted 15 May 2023; published 2 June 2023)

Attempts to unravel the nature of magnetic ordering in $LaSrCoO_4$ (Co^{3+}), a compound intermediate between antiferromagnetic (AFM) La_2CoO_4 (Co^{2+}) and ferromagnetic (FM) Sr_2CoO_4 (Co^{4+}), have met with limited success so far. In this paper, the results of a thorough investigation of dc magnetization and ac susceptibility in single-phase $LaSrCoO_4$ provide clinching evidence for a thermodynamic paramagnetic (PM)-ferromagnetic (FM) phase transition at $T_c = 220.5$ K, followed at lower temperature ($T_g = 7.7$ K) by a transition to the cluster spin glass state (CSG). Analysis of the low-field Arrott plot isotherms, in the critical region near T_c, in terms of the Aharony-Pytte scaling equation of state clearly establishes that the PM-FM transition is basically driven by random magnetic anisotropy (RMA). For temperatures below ≈ 30 K, large enough RMA destroys long-range FM order by breaking up the infinite FM network into FM clusters of finite size and leads to the formation of a CSG state at temperatures $T \lesssim 8$ K by promoting freezing of finite FM clusters in random orientations. Increasing strength of the single-ion magnetocrystalline anisotropy (and hence RMA) with decreasing temperature is taken to reflect an increase in the number of low-spin Co^{3+} ions at the expense of that of high-spin Co^{3+} ions. At intermediate temperatures ($30\ \text{K} \lesssim T \lesssim 180$ K), spin dynamics has contributions from the infinite FM network (fast relaxation governed by a single anisotropy energy barrier) and finite FM clusters (extremely slow stretched exponential relaxation due to hierarchical energy barriers).

DOI: 10.1103/PhysRevB.107.214405

I. INTRODUCTION

Low-dimensional magnetic systems are susceptible to a variety of external perturbations, such as doping, magnetic field, and strain, etc. [1]. Their higher sensitivity to external stimuli compared to the 3D counterparts opens up room for unique applications, e.g., control of exchange bias in a single unit cell [2]. Moreover, in low-dimensional systems, control of the spin moment can provide tremendous application opportunities for spintronics devices (layered cobaltates are potential candidates). $LaCoO_3$ (Co^{3+}), an often studied 3D compound, exhibits peculiar properties such as a metal-insulator transition, high-spin (HS) state to low-spin (LS) state transitions, magnetoelectronic phase separation, and ferromagnetic (FM) correlations [3]. A fascinating cobaltate and 2D analog of $LaCoO_3$ is La_2CoO_4 (Co^{2+}), an antiferromagnetic (AFM) insulator [4], but not explored enough mainly due to its topotactic oxidation [5]. Its counterpart Sr_2CoO_4 (Co^{4+}) has a similar structure and shows ferromagnetism and half-metallicity [6]. In the unit cell of $LaSrCoO_4$ (an intermediate composition of the above-mentioned end compounds), $La/SrCoO_3$ 3D blocks are separated by rock-salt La/SrO layers.

Depending upon how the energy-splitting Δ_{CF} between the t_{2g} and e_g orbitals, caused by the crystal field, compares in magnitude with the exchange energy J_{ex} associated with the Hund's rule coupling, the Co^{3+} ion can exist in three different spin states [7]: the magnetically active Co^{3+} HS ($t_{2g}^4 e_g^2$, S=2) state when $\Delta_{CF} < J_{ex}$, intermediate-spin (IS; $t_{2g}^5 e_g^1$, $S = 1$) state when $\Delta_{CF} \sim J_{ex}$ and nonmagnetic LS ($t_{2g}^6 e_g^0$, $S = 0$) state when $\Delta_{CF} \gg J_{ex}$. In the $LaSrCoO_4$ compound, the spin state of Co^{3+} ions has been a controversial issue. For instance, $LaSrCoO_4$ is reported [8–12] to have a mixture of LS and (thermally activated) HS states of the Co^{3+} ions. The presence of a homogeneous IS state of Co^{3+} ions has also been claimed [13] and subsequently challenged [14]. In our previous study [7], we probed the spin states in $La_{2-x}Sr_xCoO_4$ ($0.5 \leqslant x \leqslant 1$) compounds and found the existence of the HS and LS states together at room temperature, discarding the presence of the IS state. First-principles calculations [9] support the view that mixed spin states (HS and LS) of Co^{3+} ions inhabit the ground state of $LaSrCoO_4$.

*abdul.ahad@ntu.edu.sg; Present address: School of Physical and Mathematical Sciences, Nanyang Technological University, Singapore.
†Present address: RIKEN Center for Emergent Matter Science, Saitama, Japan.
‡Present address: National Institute of Technology, Hazratbal Srinagar J & K, India.
§Present address: Department of Physics, School of Engineering, University of Petroleum and Energy Studies, Dehradun, India.
¶sn.kaul@uohyd.ac.in
‖dkshukla@csr.res.in

The existence of mixed spin states of the Co^{3+} ions in $LaSrCoO_4$ is expected to have an important bearing on the magnetic and transport properties, since the superexchange interaction between the HS Co^{3+} ions mediated by the intervening LS Co^{3+} ion can induce long-range FM order, while the superexchange interaction between the adjacent HS Co^{3+} neighbors can give rise to AFM order. The competing FM and AFM exchange interactions, in turn, could result in a spin glass (SG) state. Conflicting reports [15–20] about the nature of magnetism in $LaSrCoO_4$, however, render the existing magnetic data inconclusive, as elucidated below. While a paramagnetic (PM)-SG transition at $T_{SG} \sim 20$ K [15] ($T_{SG} \sim 8$ K [16]) is construed as a transition from the HS to IS state, no PM-SG transition is observed down to 2 K (the temperature up to which an insulating PM state persists [18]) and a broad hump in the thermomagnetic data, observed at $\simeq 250$ K, is attributed to the FM (La,Sr)CoO_3 impurity [18]. This insulating PM ground state is taken to reflect [18] the IS spin state of Co^{3+} ions. In sharp contrast, two magnetic transitions, the PM-FM transition at $T_c \simeq 250$ K [19,20] and the SG-like transition at $T_{SG} \sim 12$ K [19] or at $T_{SG} \sim 60$ K [20], have been reported. Considering that the spin and valence states of Co are inextricably linked in cobaltates, the presence of valence states (Co^{2+} and/or Co^{4+}) of Co, arising from the varying degree of oxygen off-stoichiometry in the samples used in such investigations, could be at the root of these apparent discrepancies.

In this paper, the intrinsic magnetic behavior near the PM-FM and SG transitions is unraveled by ensuring close to a pure Co^{3+} state in our $LaSrCoO_4$ sample. DC magnetization and frequency-dependent ac susceptibility (ACS) data, unambiguously confirm the existence of two magnetic transitions: a thermodynamic (*frequency-independent*) PM-FM phase transition at $T_c = 220.5$ K and a *frequency-dependent* cluster spin glass (CSG) transition, approaching the value $T_g = 7.7$ K in the zero-frequency limit. Both of these transitions are basically driven by random magnetic anisotropy (RMA). Increasing strength of the single-ion magnetocrystalline anisotropy (and hence RMA) with decreasing temperature is shown to be a manifestation of an increase in the number of LS Co^{3+} ions at the expense of that of HS Co^{3+} ions.

II. EXPERIMENTAL METHOD

The details of sample synthesis are reported elsewhere [7]. The synchrotron x-ray diffraction (XRD) pattern was measured at room temperature using the BL-12 ADXRD beamline of RRCAT, India. To avoid possible fluorescence from Co, an x-ray photon energy of 7690 eV ($\lambda_{XRD} = 1.612$ Å), which lies below the Co K absorption edge, was used. X-ray absorption near edge spectra (XANES) were recorded in the fluorescence mode at the same beamline. The energy resolution at the Co K-edge energy was ~0.7 eV. Zero-field ($H = 0$) and in-field ($H = 80$ kOe) electrical resistivities as functions of temperature were measured by four-probe method, using the Oxford cryostat. Magnetization measurements were carried out utilizing the 7 Tesla Quantum design MPMS 3 magnetometer. $M(H)$ hysteresis loops at fixed temperatures were recorded following the field cooled

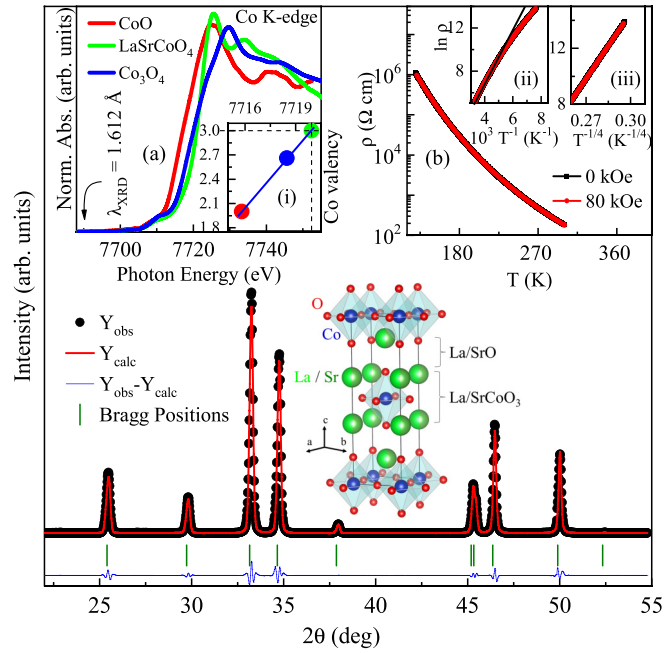

FIG. 1. Room-temperature synchrotron x-ray diffraction pattern of $LaSrCoO_4$ compound, measured at the x-ray photon energy of 7690 eV, along with the Rietveld fit. A schematic of the unit cell shows that it consists of blocks of La/$SrCoO_3$ separated by the La/SrO layers. (a) compares the Co K-edge XANES of $LaSrCoO_4$ with those of the reference compounds CoO and Co_3O_4. Linear Co valency versus Co K-edge photon energy plot in the inset (i) extrapolates to the Co valency of +3 in the $LaSrCoO_4$ compound. (b) displays the temperature variations of the zero-field [$\rho(H = 0)$] and in-field [$\rho(H = 80$ kOe)] resistivity. Insets (ii) and (iii) depict the $\ln \rho$ versus T^{-1} and $\ln \rho$ versus $T^{-1/4}$ plots, respectively.

(FC) protocol. Magnetization was measured as a function of temperature, $M(T)$, over the temperature range extending from 5 K to 300 K at fixed fields, employing the FC and zero field cooled (ZFC) protocols. The virgin $M(H)$ curves were recorded after demagnetizing the sample and the superconducting magnet by setting field to zero in the oscillatory mode. For constructing the Arrott plots from the virgin $M(H)$ isotherms, the applied field has been corrected for the demagnetizing field to arrive at the internal effective magnetic field [21] H_{eff}, in accordance with the relation, $H_{eff} = H_{applied} - (4\pi N)\, M$, where N is the demagnetizing factor, which was determined from the low-field portions of the $M(H)$ isotherms taken at $T < T_c$. The ZFC relaxation measurement was performed by cooling the sample down to 150 K in zero field and, after waiting for 100 s (t_w), a static magnetic field of 50 Oe was applied and the time evolution of magnetization at 150 K was measured up to ~ 8000 s. The real [$\chi'(\omega, T)$] and imaginary [$\chi''(\omega, T)$] components of ac magnetic susceptibility were measured in the temperature range of 2–300 K at fixed frequencies (1.1 Hz–941 Hz) of the ac driving field of rms amplitude, $h_{ac} = 3$ Oe employing the Quantum Design MPMS 3 system equipped with an ACS option.

III. RESULTS AND DISCUSSION

Figure 1 shows the room-temperature synchrotron XRD pattern of the $LaSrCoO_4$ compound together with the

Rietveld fit. The absence of any extra Bragg peak, confirms the single-phase nature of the $LaSrCoO_4$ sample. Rietveld refinement yielded the lattice parameters, corresponding to the tetragonal space group $I4/mmm$, as $a = 3.8025(3)$ Å and $c = 12.4985(2)$ Å. Figure 1(a) compares the Co K-edge XANES data of $LaSrCoO_4$ with those of the reference compounds CoO and Co_3O_4. Linear Co valency versus Co K-edge photon energy plot in inset (i) yields the value +2.98(2) for the Co valence and thereby confirms the Co valency of +3 in the $LaSrCoO_4$ sample. Data points, depicted by circles in the linear plot shown in Fig. 1(a)(i), correspond to the first derivative of the absorption edges.

Figure 1(b) clearly demonstrates semiconducting-like temperature variation of the zero field [$\rho(H = 0)$] and in-field [$\rho(H = 80$ kOe)] resistivity in the $LaSrCoO_4$ sample. If, apart from Co^{3+} ions, Co^{2+} and Co^{4+} ions were also present in the sample, double exchange, involving charge hopping, would have resulted in a metallic state (characterized by low resistivity, typically ∼10–100 μΩ cm, and ρ increasing with temperature) as opposed to the observed semiconducting-like state with very large resistivity decreasing from 10^6 Ω cm at 130 K to 10^2 Ω cm at 310 K. Consistent with the conclusion drawn from the Co K-edge XANES data, this finding completely rules out the presence of Co^{2+} and Co^{4+} ions in our sample. Furthermore, negligibly small magnetoresistance (MR), $[(\rho(T,H = 80$ kOe$)-\rho(T,H = 0)]/\rho(T,H = 0)$, observed in the present case, sharply contrasts the reasonably large negative MR expected in double-exchange ferromagnets. Figures 1(b)(ii) and 1(b)(iii) bear out clearly that the processes such as the thermal activation of charge carriers across the band gap (described by expression $\rho \sim e^{E/k_BT}$) and Mott variable-range polaron hopping (represented by the expression $\rho \sim e^{(T_0/T)^{1/4}}$) [22–24] operate within the temperature ranges 225 K–300 K ($T > T_c$) and 130 K–220 K ($T \leqslant T_c$), respectively.

After ensuring that the sample is of very good quality (free from the impurity phases), in the following, we attempt to unravel the *intrinsic* magnetic behavior of the $LaSrCoO_4$ compound. Figure 2(a) displays the FC and ZFC thermomagnetic curves, $M(T)$, at fixed magnetic fields in the range 10 Oe–10 kOe. A clear bifurcation between FC and ZFC $M(T)$ is observed at low fields. Such bifurcations are indicative of either a SG phase [25] or CSG phase or magnetic anisotropy energy barriers or superparamagnetism [26]. A closer look at the low-temperature ZFC $M(T)$ data shows a clear cusp [Fig. 2(b)] at $T_g \sim 8$ K. A similar feature was observed previously [16,17,19] and denoted as a freezing temperature. An interesting point to note is that on cooling below $T_{\rm Irr}$ [the temperature at which FC and ZFC $M(T)$ bifurcate], M_{FC} increases, which is taken to be a characteristic feature of CSG behavior in various systems [27]. The increase in M_{FC} with decreasing temperature, even below T_g, points to the presence of a CSG state [28] because M_{FC} normally exhibits a plateau for canonical spin glass [29]. It is noteworthy to mention that, for typical re-entrant SG systems, the irreversibility occurs far below T_c while for CSG $T_{\rm Irr} \leqslant T_c$ [30]. In this connection, it is also reported [3] that if the bifurcation temperature $T_{\rm Irr} \gg T_g$, the compound exhibits CSG-type behavior while, for canonical SG [31], the $T_{\rm Irr}$ coincides with the T_g. Thus, we

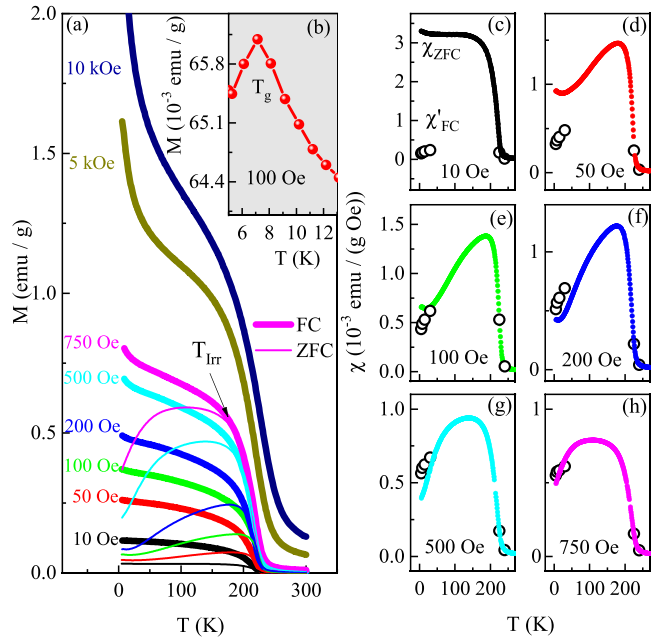

FIG. 2. (a) Thermomagnetic $M(T)$ curves taken at fixed magnetic fields. (b) shows the enlarged view of ZFC $M(T)$ at low temperatures which facilitates the observation of the spin glass transition at T_g. (c)–(h) Temperature variations of the susceptibilities measured (solid circles) and calculated (open circles) at the different fixed magnetic fields.

conclude that the signatures discussed above basically reflect the CSG state in $LaSrCoO_4$ at low temperatures.

Next, we discuss the role of magnetic anisotropy as a possible source of bifurcation in $M(T)$. Because of the prevalent elongated octahedra in the crystal structures similar to that in the $LaSrCoO_4$, the pseudo-orbital moment of Co^{3+} HS, $\tilde{L} = 1$ [32], prefers to lie in plane and forces the spin moment also to lie within the plane [33] due to the spin-orbit coupling. Neutron diffraction studies on isostructural compounds $LaSrFeO_4$ [34] and half-doped $La_{1.5}Sr_{0.5}CoO_4$ [35] have clearly borne out that, in these systems, magnetic moments are confined to the *ab* plane but can rotate within the plane. This is indicative of an XY-type anisotropy and hence the *c* axis may not be the easy axis of magnetization. To ascertain whether or not magnetic anisotropy plays a role, we adopted the approach proposed by Joy *et al.* [26], according to which, if the decrease in M_{ZFC} at low temperatures is due to magnetocrystalline anisotropy, M_{ZFC} should follow the relation, $\frac{M_{FC}}{H_{app}+H_c} \approx \frac{M_{ZFC}}{H_{app}}$. That this is indeed the case for the fields $H \geqslant 100$ Oe, is evident from Figs. 2(e)–2(h). However, at $H \leqslant 50$ Oe, χ_{ZFC} $(= \frac{M_{ZFC}}{H_{app}})$ strongly deviates from χ'_{FC} $(= \frac{M_{FC}}{H_{app}+H_c})$ [see Figs. 2(c) and 2(d)] in the low-temperature region. The demagnetization-limited behavior of χ_{ZFC} at $T < T_c$ for $H = 10$ Oe, suggests that the shape anisotropy also becomes important at low fields $H \leqslant 50$ Oe. Note that, in the calculation of χ'_{FC}, we have used the coercive field, $H_c(T)$, data shown in the inset of Fig. 3.

Figure 3 presents the $M(H)$ hysteresis loops at fixed temperatures, taken in the FC (H = 70 kOe) mode at temperatures below and above the PM-FM transition temperature, $T_c =$

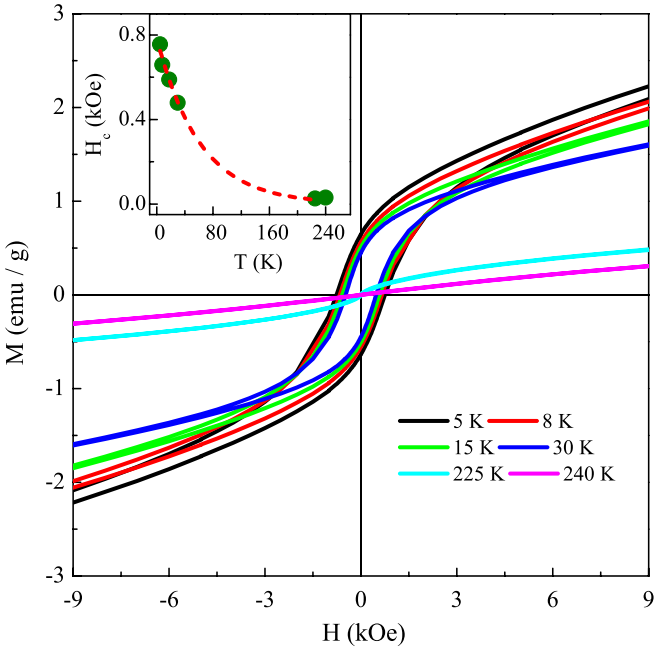

FIG. 3. Field-cooled $M(H)$ hysteresis loops. Inset shows the variation of H_c with temperature.

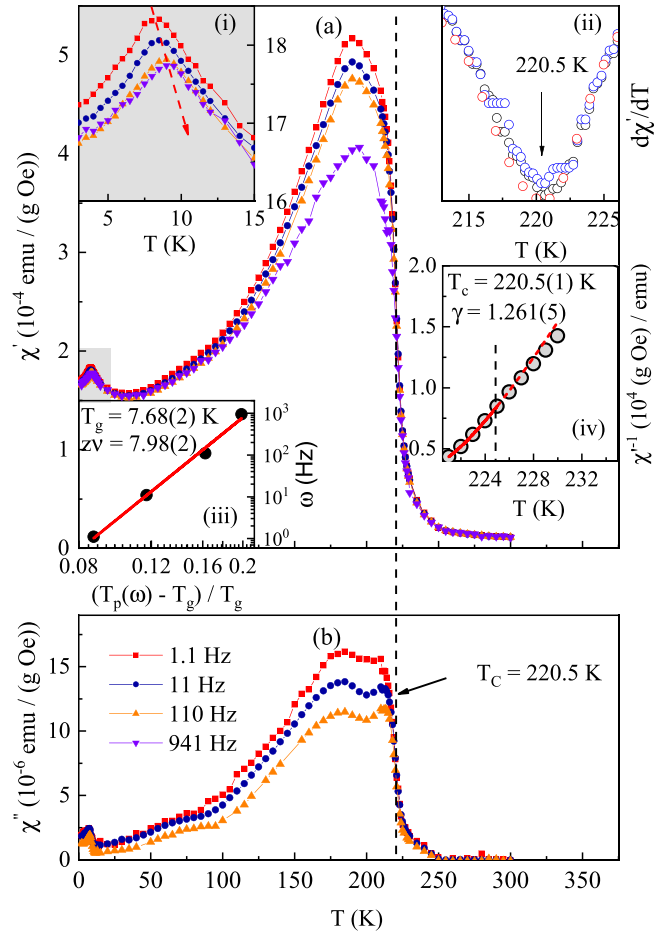

FIG. 4. Temperature dependence of (a) in-phase component, χ', and (b) out-of-phase component, χ'' of χ_{ac} at the different frequencies (1.1 to 941 Hz) measured at an ac driving field of rms amplitude 3 Oe. Inset (i) of panel (a) shows a zoomed view of the frequency dependence of the peak in χ'(T) at around $\sim$ 8 K while inset (ii) depicts the $d\chi'/dT$ versus T at different frequencies. The linear fit through the ω versus $(T_p(\omega) - T_g)/T_g$ data (solid circles) in inset (iii) testifies to the validity of the critical slowing-down model. Inset (iv) displays the fit (red curve) to the inverse ac susceptibility, $\chi'^{-1}(T)$, data (open circles) above $T_c = 220.5$ K in the range 221 K–225 K, based on Eq. (2). This fit, when extended to 230 K (dashed curve), demonstrates that the $\chi'^{-1}(T)$ data start deviating from the fit for $T > 225$ K.

220.5 K, (corresponding to the dip in $dM_{ZFC}(T)/dT$ at low fields H = 10–100 Oe, not shown here). With temperature decreasing from $T \gg T_c$, where the sample is in the PM state and as such the $M(H)$ isotherms are linear, the coercive field, H_c, increases from zero at $T = T_c = 220.5$ K to about 800 Oe at 5 K; the rate of increase in H_c picks up for temperatures below 30 K, as is evident from the inset of Fig. 3. A steep increase in H_c as the temperature falls below 30 K is indicative of an increase in the RMA [presence of RMA is inferred from the critical-point (CP) analysis in the following section]. The observation that magnetization does not saturate even in fields as high as 70 kOe at low temperatures [Fig. 5(a)] and the presence of RMA support the existence of a CSG state at low temperatures.

Figures 4(a) and 4(b) display the temperature variations of the real (χ') and imaginary (χ'') parts of ac magnetic susceptibility, respectively. While Fig. 4(a)(i) highlights the frequency-induced shift in the peak in $\chi'(T)$ at $T = T_p \simeq$ 8 K, the Fig. 4(a)(ii) clearly brings out the frequency independence of the dip in the $d\chi'/dT$ versus T plots at $T_c =$ 220.5 K, which corresponds to the inflection point in $\chi'(T)$. The frequency-independent value of $T_c = 220.5$ K confirms the true thermodynamic nature of the FM-PM phase transition at T_c.

The shift in T_p per decade of frequency $(\Delta T_p/\{T_p \Delta(\log_{10}\omega)\} = 3.2\times10^{-2})$ is an order of magnitude greater than that ($\simeq 10^{-3}$) observed [31] in canonical SGs but is typical of the CSGs [31,36]. The frequency dependence of the peak temperature, $T_p(\omega)$, is analyzed in terms of the following expression given by the critical slowing down model [31,36]:

$$\omega = \omega_0 \left[\frac{T_p(\omega) - T_g}{T_g}\right]^{z\nu}, \qquad (1)$$

where $\tau_o = 2\pi/\omega_0$ is the relaxation time due to the correlated spin dynamics, T_g is the SG transition temperature in the zero-frequency limit, ν is the spin-spin correlation length critical exponent, and z is the dynamical critical exponent. The linear fit through the ω versus $(T_p(\omega) - T_g)/T_g$ data (solid circles) in Fig. 4(a)(iii), based on Eq. (1) with the parameter values $\tau_o = 2.49(1)\times10^{-8}$ s, $T_g = 7.68(2)$ K and the product $z\nu =$ 7.98(2), testifies to the validity of the critical slowing down model. Note that, in the canonical SGs, relaxation time, τ_o, is typically of the order of 10^{-12} s [31,36]. Several orders of magnitude larger τ_o (i.e., much slower spin dynamics), in the present case, further confirms the existence of a CSG ground state.

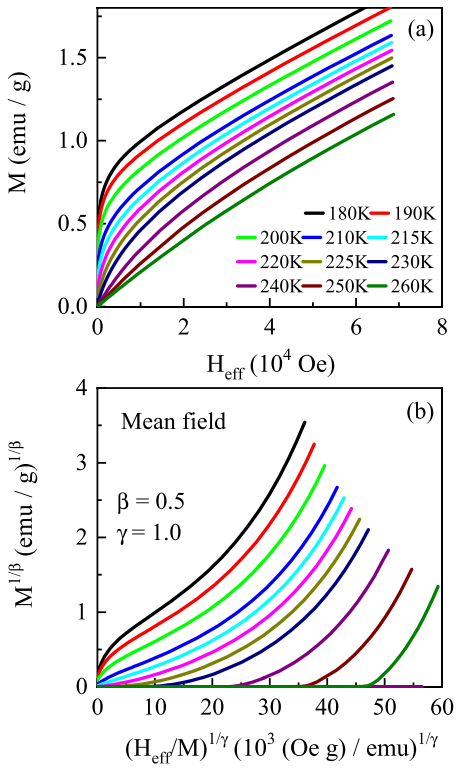

FIG. 5. (a) $M(H)$ isotherms around T_c. (b) The modified Arrott [$M^{1/\beta}$ versus $(H/M)^{1/\gamma}$] plots with the choice of the critical exponents β and γ given by the mean-field theory.

Next, we focus our attention on the FM-PM transition at $T_c = 220.5$ K. In the critical region above T_c, the inverse of measured ACS, $\chi_{ac}^{-1}(T) \equiv \chi'^{-1}(T)$, is related to the inverse intrinsic susceptibility, $\chi_{int}^{-1}(T)$ as $\chi_{ac}^{-1}(T) = 4\pi\ N + \chi_{int}^{-1}(T)$, where N is the demagnetizing factor. As the temperature approaches T_c from above, χ_{int} diverges (or equivalently, χ_{int}^{-1} goes to zero) at T_c in accordance with the relation

$$\chi_{ac}^{-1}(T) = 4\pi N + A\left[\frac{T - T_c}{T_c}\right]^{\gamma}, \tag{2}$$

where A and γ are the critical amplitude and critical exponent, respectively. Figure 4(a)(iv) depicts the best theoretical fit (continuous curve) to the $\chi_{ac}^{-1}(T)$ data, based on the Eq. (2), yields $T_c = 220.5$ K, $A = 5.9(1)\times10^5$ and $\gamma = 1.261(5)$. This value of γ will be put into a proper context later in the text.

It is well-known that the CP analysis of magnetization, $M(T,H)$, data taken in the critical region near T_c provides a powerful means to unravel the true nature of magnetic ordering prevalent in a spin system. As elucidated below, the CP analysis makes use of the critical exponents β, γ, and δ for the spontaneous magnetization (order parameter), ZF susceptibility, and the critical $M(H)$ isotherm, (characterizing a continuous FM-PM phase transition at T_c), that are defined as [37]

$$M_s = B\ |\epsilon|^{\beta} \quad T < T_c, \quad H \to 0, \tag{3}$$

$$\chi_0 = A\ \epsilon^{-\gamma} \quad T > T_c, \quad H \to 0 \tag{4}$$

$$M = M_0\ H^{1/\delta} \quad T = T_c, \tag{5}$$

where $\epsilon = (T - T_c)/T_c$, A, B, and M_0 are the critical amplitudes [37,38]. Diverse systems having exactly the same values for the critical exponents β, γ, and δ, fall into a single universality class. The universality class, in turn, is governed by the order parameter (spin) dimensionality (n) and spatial dimensionality (d) [37,39] as long as the interaction coupling the spins is of short range. The presence of different valence and spin states in the present system is expected to have a profound effect on the critical behavior. This expectation called for a detailed study of the critical behavior of $LaSrCoO_4$ at temperatures in the vicinity of the FM-PM phase transition. To this end, we have analyzed the virgin $M(H)$ isotherms in the critical region [shown in Fig. 5(a)] using the scaling equation of state (SES) method, detailed in Ref. [37]. Instead of following the customary practice of using, at first, the Arrott [40] SES, we use the generalized form of the Arrott SES, given by Arrott and Noakes [41] (AN), i.e.,

$$(H/M)^{1/\gamma} = a[(T - T_c)/T_c] + bM^{1/\beta}, \tag{6}$$

to arrive at the correct choice of the critical exponents that makes the AN, $M^{1/\beta}$ versus $(H/M)^{1/\gamma}$, plots a set of parallel straight lines in the critical region near T_c. The temperature at which the linear AN plot isotherm passes through the origin marks the T_c. To begin, we ascertain if the values of critical exponents β and γ, theoretically predicted for any universality class, make the AN plot isotherms at temperatures close to T_c linear. For example, in Fig. 5(b), it is evident that the mean-field (MF) critical exponent values $\beta = 0.5$ and $\gamma = 1$ do not yield linear AN isotherm in the critical region. The data presented in Fig. S1 of the Supplemental Material [42] demonstrate that, like the MF critical exponent values, none of the universality class critical exponent choices: $\beta = 0.365$, $\gamma = 1.386$ for three-dimensional (3D) Heisenberg; $\beta = 0.345$, $\gamma = 1.316$ for 3D-XY; $\beta = 0.325$, $\gamma = 1.241$ for 3D Ising and $\beta = 0.25$, $\gamma = 1.0$ for MF tricritical, results in the linear AN plot isotherms.

Furthermore, regardless of the choice of the critical exponents β and γ, extrapolation of the high-field portions of the AN isotherms to $H = 0$ does not give any intercept on the $M^{1/\beta}$ axis. No intercept on the ordinate axis implies no spontaneous magnetization and hence absence of long-range FM order. This result prompted us to look for even the nonuniversal exponent values that could lead to the desired linear AN plot isotherms.

By varying the values of β and γ in Eq. (6), we succeeded in making the AN plot isotherms nearly straight over the field range 1.5 kOe $\lesssim H \lesssim$ 10 kOe with the critical exponent values, $\beta = 0.796$, $\gamma = 1.051$. Note that the field range for the linear AN isotherms is much wider in the immediate vicinity of T_c. From the modified Arrott plot (Fig. 6), it is evident that the extrapolation of the linear portions of the AN isotherms to $H = 0$ yields finite spontaneous magnetization, M_s, (inverse susceptibility, χ^{-1}) below (above) T_c, and both M_s and χ^{-1} are zero at the transition temperature $T_c \simeq 220$ K. This value of T_c is very close to that deduced from the ACS data. Using the critical exponent values, $\beta = 0.796$ and $\gamma = 1.051$, in the Widom scaling relation [43] $\delta = 1 + \gamma/\beta$, we obtained the critical isotherm critical exponent δ as 2.32. To crosscheck this value, the relation [Eq. (5)] is used to fit the virgin $M(H)$

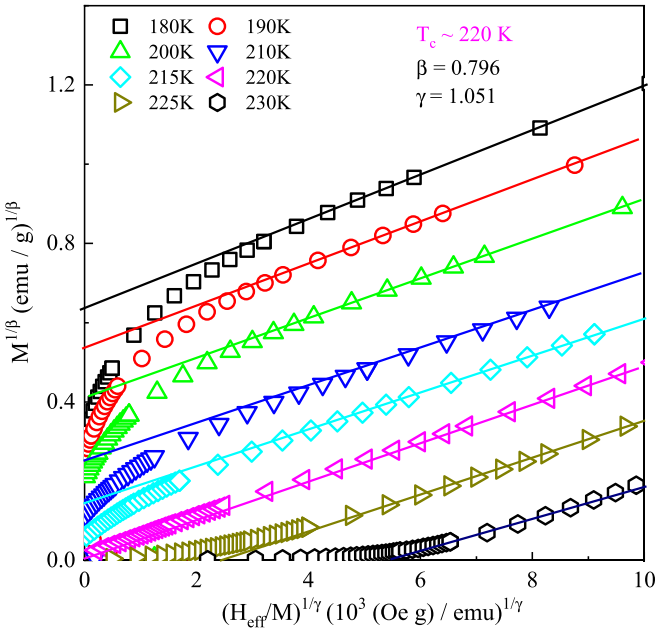

FIG. 6. Arrott plots constructed using the critical exponent values $\beta = 0.796$ and $\gamma = 1.051$.

isotherm at $T_c \simeq 220$ K. Figure 7(c) shows the critical $M(H)$ isotherm plotted as the ln M versus ln $H_{\rm eff}$ plot. As expected from Eq. (5), this log-log plot is linear with inverse slope

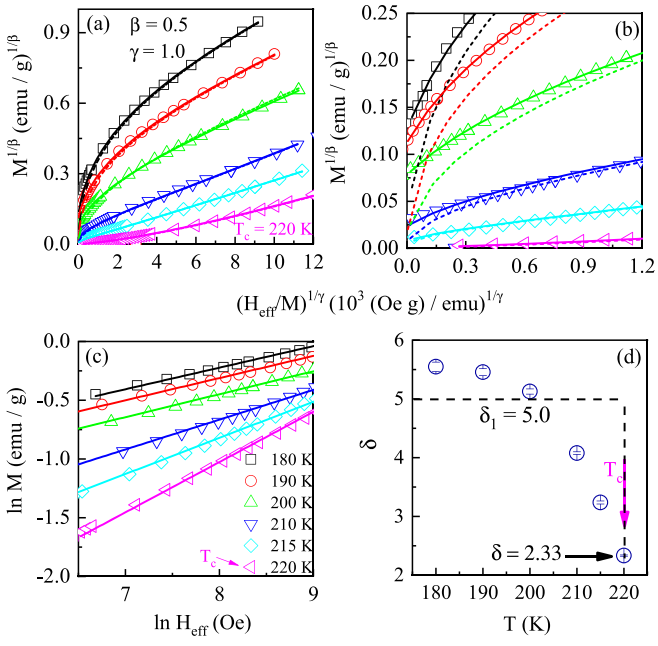

FIG. 7. (a) Theoretical fits to the Arrott plot [i.e., $M^{1/\beta}$ versus $(H/M)^{1/\gamma}$ plot with mean-field exponents $\beta = 0.5$ and $\gamma = 1$] isotherms, based on the scaling equation of state, Eq. (8), predicted by the random anisotropy model. (b) Enlarged view of the data and fits at fields nearing zero. (c) The linear ln M versus ln $H_{\rm eff}$ plots at $T \leqslant T_c$. (d) Critical exponent δ_1 at different temperatures below T_c and the critical exponent δ at T_c, obtained from the linear fits to the ln M versus ln $H_{\rm eff}$ data shown in (c).

$\delta = 2.35(5)$. This value of δ is in excellent agreement with that obtained using the Widom scaling relation.

Despite a close agreement between the value of δ directly determined from the critical isotherm and that from the exponent values $\beta = 0.796$ and $\gamma = 1.051$ via the Widom scaling relation, two basic questions arise: (i) How does one reconcile with the nonuniversal critical exponent values and (ii) what causes the deviations from the linear AN isotherms at sufficiently low fields? Considering that the RMA model [44] yields nonlinear MF AN isotherms at low fields, it is worth investigating if the SES form given by Aharony and Pytte (AP) [44] helps resolve the above issues. Note that nonlinear MF isotherms have been observed in the past in a number of amorphous rare earth–transition metal systems and explained [45] in terms of the AP model.

Neglecting the critical fluctuations, AP made the following predictions for a (d, n) spin system with RMA. (I) The $M(H)$ isotherms follow the relation $H \sim M^{1/\delta}$ at T_c and $H \sim M^{1/\delta_1}$ at all temperatures below T_c, with the exponents δ and δ_1 given by

$$\delta = \frac{10 - d}{6 - d}, \quad \delta_1 = \frac{8 - d}{4 - d}. \tag{7}$$

For a three-dimensional ($d = 3$) system, Eqs. (7) gives $\delta = 7/3 = 2.33$ and $\delta_1 = 5.0$. While the theoretical estimate $\delta = 2.33$ is in perfect agreement with the presently determined value $\delta = 2.35(5)$, the observed δ_1 values do not reproduce the theoretically predicted abrupt jump in δ_1 at $T \simeq T_c$ to the value $\delta_1 = 5.0$, which remains constant for $T < T_c$ [as evidenced in Fig. 7(d)]. This discrepancy between theory and experiment can be traced back to a total neglect of critical fluctuations of the order parameter, leading to Eqs. (7). (II) According to the AP model, the SES has the following form [44] for a $d = 3$, $n = 3$ system with random uniaxial and cubic anisotropies:

$$M^{1/\beta} = \left[\left(\frac{H}{M}\right)^{1/\gamma} - a\frac{(T - T_c)}{T_c}\right] \Bigg/ b\left[1 + c\left(\frac{H}{M} + 4\,\kappa\, M^2\right)^{-1/2}\right], \tag{8}$$

where $\beta = 0.5$, $\gamma = 1.0$, and $c \sim (D/J)^2$; D, and κ are a measure of random uniaxial and cubic anisotropies, respectively, and J signifies the exchange interaction. Equation (8) permits a clear distinction between the cases: (i) $\kappa = 0$ when only the random uniaxial anisotropy exists and (ii) $\kappa \neq 0$ when, in addition to the random uniaxial anisotropy, cubic anisotropy is present. The low-field $M_T(H)$ data, plotted in the form of the Arrott plot [i.e., $M^{1/\beta}$ versus $(H/M)^{1/\gamma}$ plot with MF exponents $\beta = 0.5$ and $\gamma = 1$] isotherms, and the theoretical fits based on the AP SES, Eq. (8), for the cases $\kappa = 0$ (dashed curves) and $\kappa \neq 0$ (continuous curves), are displayed in Fig. 7(a). Figure 7(b) provides an enlarged view of the data and fits at fields not very far from zero. Evidently, the AP SES correctly reproduces the observed change in the curvature of the Arrott plot isotherms from concave downward to concave upward at T_c. Furthermore, superiority of the $\kappa \neq 0$ fits over those corresponding to $\kappa = 0$, particularly at fields close to zero, asserts that the inclusion of cubic anisotropy is necessary. Consequently, in

conformity with the observed behavior, an extrapolation to $H = 0$ gives finite intercepts on the ordinate (finite M_s) for $T < T_c$ and on the abscissa (finite χ^{-1}) for $T > T_c$; both M_s and χ^{-1} go to zero at $T = T_c$. However, due to sizable gradients of the AP isotherms at very low fields ($H \to 0$) for temperatures on either side of T_c, the intercepts on the ordinate and abscissa depend on the range of H chosen for extrapolation. Thus, the $M_s(T)$ and $\chi^{-1}(T)$, so obtained, are not accurate enough for the determination of critical exponents β and γ. In sharp contrast, the ZF ACS does not suffer from such extrapolation errors. The value $\gamma = 1.261(5)$ of the susceptibility critical exponent, determined from the ACS data, is thus reliable. The deviation of this value of γ from the MF value, $\gamma = 1.0$, underscores the importance of critical fluctuations (neglected in the AP RMA model). Thus, the RMA model, due to AP [44], captures the main physical essence in that the curvature in the MF Arrott isotherms at low fields has its origin in the random uniaxial and cubic anisotropies but fails to yield correct values for the critical exponents β and γ.

The evidence presented so far asserts that (i) at temperatures in range 180 K $\leqslant T \leqslant$ $T_c = 220.5$ K, RMA is too weak to destroy long-range FM order, and (ii) the transition to a CSG state occurs at $T_g = 7.7$ K. It remains to be verified if, in the intermediate temperature range, a mixed state is formed in which long-range FM order coexists with the CSG order. In this connection, Fig. 8(a) makes it obvious that, in the low-temperature region ($T \lesssim 30$ K), the Arrott (M^2 versus H/M) plots, when extrapolated to $H = 0$, do not yield any intercept on the ordinate axis regardless of the field-range chosen for extrapolation. It immediately follows that no spontaneous magnetization, and hence no long-range FM order, exists at these temperatures. Concurrently, in the same temperature range $T \lesssim 30$ K, a steep rise in RMA (reflected in a sharp increase in the coercive field, as noticed in the inset of Fig. 3) occurs. Within the framework of the RMA models [44,46], the sizable magnitude of RMA at $T \lesssim 30$ K can account for both the breakdown of long-range FM order [44] and the freezing of spin clusters in random orientations at $T = T_g$, leading to the formation of a cluster (correlated) SG state (with a finite FM correlation length [46]) at temperatures below T_g.

With a view to gain more insight into the nature of magnetism at temperatures intermediate between the SG transition temperature $T_g \simeq 8$ K and $T_c \simeq 220.5$ K, the time (t) evolution of the ZFC magnetization, $M_{\rm ZFC}(t)$, at 150 K was measured in a static magnetic field of 50 Oe (switched on after a fixed waiting time, t_w, ranging between 10^2 and 10^4 s). The $M_{\rm ZFC}(t)$ data, so obtained, were fitted to the stretched exponential function given by expression

$$M(t) = M_0 - M_r \exp(-(t/t_r)^x), \tag{9}$$

where M_0 represents the FM component while M_r and t_r are the SG magnetization component and the characteristic SG relaxation time, respectively [47]. The value of exponent x reflects the type of energy barriers present. For instance, $x = 1$ describes the relaxation behavior of a FM system with a single anisotropy energy barrier separating the ZFC and FC states [48]. $x \simeq 0.5$, on the other hand, is associated with the stretched exponential relaxation, caused by hierarchical energy barriers in SGs [31]. From the fit (solid red curve through the data points), based on the above expression [Eq. (9)], to the

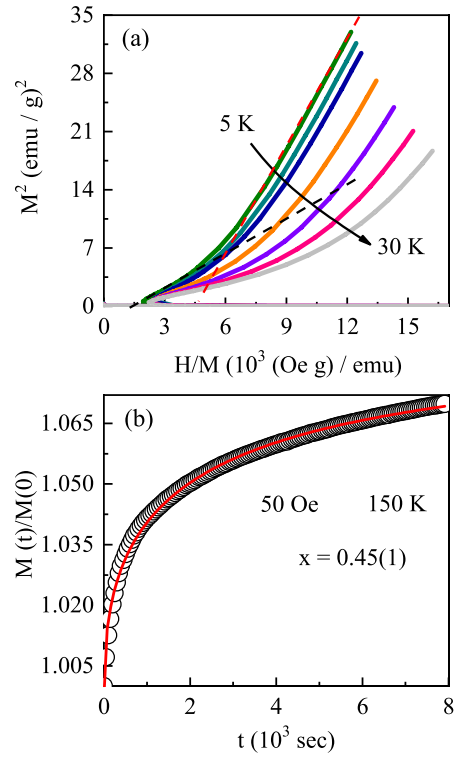

FIG. 8. (a) M^2 versus (H/M) plots in the low (5–30 K) temperature region demonstrate that no spontaneous magnetization, M_s, exists at such temperatures. (b) Time evolution of the ZFC magnetization, $M(t)$, at 150 K measured in a static magnetic field of 50 Oe switched on with a time delay of 100 s. Note that $M(t)$ is normalized to its value at the time when the field was applied. The solid red curve through the data points (open circles) represents the fit to the stretched exponential function.

$M(t)/M(0)$ data [Fig. 8(b)], we obtain $x = 0.45(1)$, $M_0/M(0) = 1.083(1)$, $M_r/M(0) = 0.086(1)$ and $t_r = 2252$ sec, where $M(0) = 1.0348$ is magnetization value, recorded at the time t_w when the field was applied. The determined value of x is in good agreement with those generally reported for SG systems [31]. This result provides evidence of the coexistence of a glassy (a cluster SG-like) phase with FM order at intermediate temperatures. Note that, within the uncertainty limits, the above-mentioned parameter values seem to be insensitive to the choice of t_w, presumably because M_r constitutes a tiny fraction of the total magnetization at the measurement temperature of 150 K, which lies well above $T_g \simeq 8$ K.

Finally, an attempt is made to ascertain how the present results can be understood in terms of the HS/IS/LS spin states of Co^{3+} ions in the $LaSrCoO_4$ compound. First, we recall that the single-ion magnetocrystalline anisotropy (MCA) has its origin in the combined action of the crystal-field interaction (CFI) and spin-orbit coupling (SOC). Since the LS state is associated with $S = 0$, the LS Co^{3+} ions, neither in isolation nor as neighbors, contribute to spin magnetic moment and MCA (due to the lack of SOC). However, in the case of LS Co^{3+} ions with HS neighbors, the spin-state configurations, fluctuating [11,12] between the Co^{3+} HS – O^{2-} – Co^{3+} LS – O^{2-} – Co^{3+} HS and Co^{3+} IS – O^{2-} – Co^{3+} HS – O^{2-} – Co^{3+} IS configurations (refer to the schematic diagram shown in

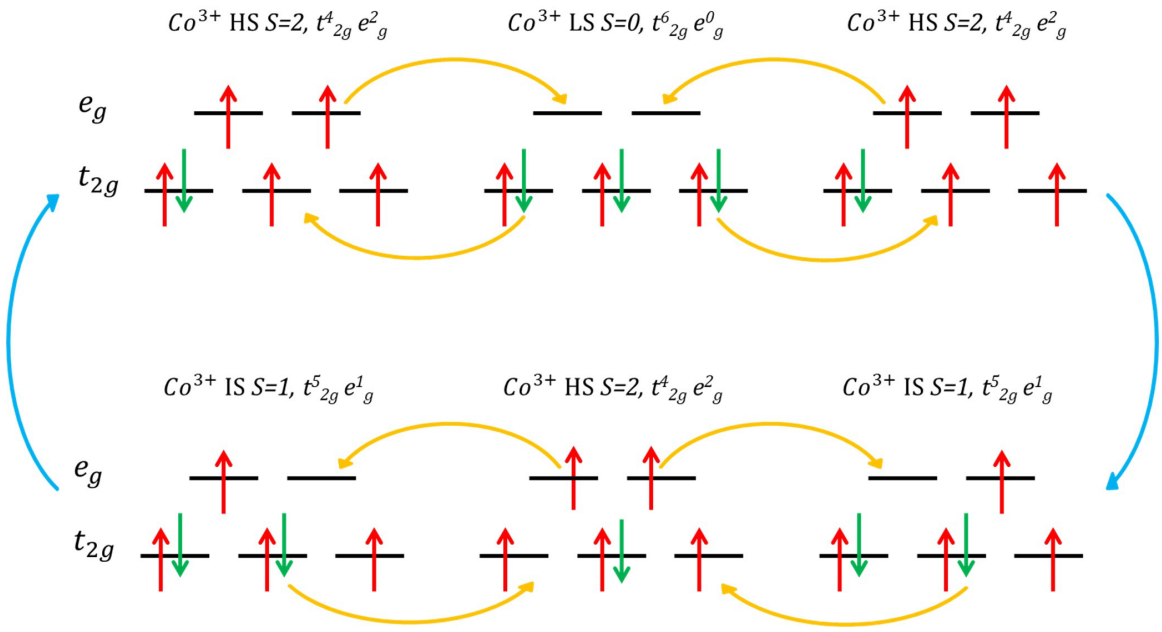

FIG. 9. Schematic showing the two interchangeable spin state configurations involving correlated hopping of t_{2g} and e_g electrons between the HS and LS states in the ground state and HS and IS states in the excited state.

Fig. 9), can lead to FM superexchange interaction between the spins of Co^{3+} HS ions. This process involves correlated hopping [11,12] of t_{2g} and e_g electrons between Co^{3+} LS and its Co^{3+} HS neighbors without any charge transfer as shown in Fig. 9 and results in a finite effective S at the LS Co^{3+} ion site. Finite S, in turn, enables SOC and ensures a significant contribution to spin magnetic moment. In conformity with the observed steep rise in MCA as the temperature drops below ~80 K, MCA increases with decreasing temperature because LS Co^{3+} ions with SOC and much stronger CFI (and hence MCA) increase [11,12,49] in number at the expense of HS Co^{3+} ions. In sharp contrast, arguments based on the mixed HS-IS or IS ground state (similar to those presented above), at best, lead to a much slower increase in MCA with lowering temperature because of their low CFI relative to LS. A competition between the above-mentioned FM interaction and the AFM interaction between the spins of neighboring Co^{3+} HS ions, caused by the Co^{3+} HS – O^{2-} – Co^{3+} HS superexchange, give rise to a SG ground state.

IV. SUMMARY AND CONCLUSION

In the $LaSrCoO_4$ compound, as functions of temperature, ZFC dc susceptibility, $\chi_{dc} = M/H$, at low fields ($H \leqslant 100$ Oe), and ACS, χ_{ac}, at different frequencies of the driving ac field of rms amplitude $h_{ac} = 3$ Oe, exhibit peaks at around 200 K and 8 K. While the low-temperature peak in $\chi_{ac}(T)$ shifts to higher temperatures with increasing frequency, the inflection-point in $\chi_{ac}(T)$ (or equivalently, a dip in $d\chi_{ac}/dT$) at 220.5 K is frequency independent. Note that the dip in $d\chi_{dc}/dT$ also occurs at exactly the same temperature. This observation provides strong experimental evidence for the existence of a thermodynamic PM-FM phase transition at $T_c = 220.5$ K. The frequency-induced shift in the low-temperature peak is described well by the critical slowing down model for a CSG. According to this model, the transition to the CSG state takes place at $T_g = 7.7$ K in the zero-frequency limit. The AP model for a ($d = 3$, $n = 3$) Heisenberg spin system with RMA yields the value ($\delta = 7/3$) of the critical exponent for the critical isotherm at $T_c = 220.5$ K, which agrees closely with the observed value of $\delta = 2.35(5)$. Moreover, the AP SES correctly describes the observed crossover from the concave-downward to concave-upwards curvature in the low-field Arrott plot isotherms, as the temperature is increased through T_c. These findings clearly establish that the PM-FM transition is basically driven by RMA.

For temperatures below $\approx$ 30 K, large enough RMA destroys long-range FM order by breaking up the infinite FM network into FM clusters of finite size and leads to the formation of a CSG state at temperatures $T \lesssim 8$ K by promoting freezing of finite FM clusters in random orientations. Increasing strength of the single-ion magnetocrystalline anisotropy (and hence RMA) with decreasing temperature reflects an increase in the number of LS Co^{3+} ions at the expense of that of HS Co^{3+} ions. At intermediate temperatures (30 K $\lesssim T \lesssim$ 180 K), spin dynamics has contributions from the infinite FM network (fast relaxation governed by a single anisotropy energy barrier) and finite FM clusters (extremely slow stretched exponential relaxation due to hierarchical energy barriers).

ACKNOWLEDGMENTS

The authors acknowledge K. Sharma for AC susceptibility measurements. S.S.M. acknowledges the financial support from SERB, India, in the form of the national postdoctoral fellowship (NPDF) award (No. PDF/2021/002137). R.S. acknowledges the financial support provided by the Ministry of Science and Technology in Taiwan under Projects No. MOST-111-2124-M-001-009, No. MOST-110-2112-M-001-065-MY3, and No. AS- iMATE-111-12.

[1] C. Gong and X. Zhang, Two-dimensional magnetic crystals and emergent heterostructure devices, Science **363**, eaav4450 (2019).

[2] A. Ahad, K. Gautam, K. Dey, S. S. Majid, F. Rahman, S. K. Sharma, J. A. H. Coaquira, I. da Silva, E. Welter, and D. K. Shukla, Magnetic correlations in subsystems of the misfit $[Ca_2CoO_3]_{0.62}$ $[CoO_2]$ cobaltate, Phys. Rev. B **102**, 094428 (2020).

[3] J. Wu and C. Leighton, Glassy ferromagnetism and magnetic phase separation in $La_{1-x}Sr_xCoO_3$, Phys. Rev. B **67**, 174408 (2003).

[4] R. A. M. Ram, P. Ganguly, and C. N. R. Rao, Preparation and characterization of La_2CoO_4, Mater. Res. Bull. **23**, 501 (1988).

[5] A. Nemudry, P. Rudolf, and R. Schollhorn, Room temperature topotactic oxidation of lanthanum cobalt oxide La_2CoO_4, Solid State Ionics **109**, 213 (1998).

[6] P. K. Pandey, R. J. Choudhary, and D. M. Phase, Magnetic behavior of layered perovskite Sr_2CoO_4 thin film, Appl. Phys. Lett. **103**, 132413 (2013).

[7] A. Ahad, D. K. Shukla, F. Rahman, S. S. Majid, Tarachand, G. S. Okram, A. K. Sinha, and D. M. Phase, Colossal thermopower, spin states and delocalization effects in single layered $La_{2-x}Sr_xCoO_4$, Acta Mater. **135**, 233 (2017).

[8] J. Wang, W. Zhang, and D. Y. Xing, Magnetic structure of the layered perovskite $LaSrCoO_4$, Phys. Rev. B **62**, 14140 (2000).

[9] H. Wu, High-spin and low-spin mixed state in $LaSrCoO_4$: An ab initio study, Phys. Rev. B **81**, 115127 (2010).

[10] N. Hollmann, M. W. Haverkort, M. Cwik, M. Benomar, M. Reuther, A. Tanaka, and T. Lorenz, Anisotropic susceptibility of $La_{2-x}Sr_xCoO_4$ related to the spin states of cobalt, New J. Phys. **10**, 023018 (2008).

[11] M. Merz, P. Nagel, C. Pinta, A. Samartsev, H. v. Löhneysen, M. Wissinger, S. Uebe, A. Assmann, D. Fuchs, and S. Schuppler, X-ray absorption and magnetic circular dichroism of $LaCoO_3$, $La_{0.7}Ce_{0.3}CoO_3$, and $La_{0.7}Sr_{0.3}CoO_3$ films: Evidence for cobalt-valence-dependent magnetism, Phys. Rev. B **82**, 174416 (2010).

[12] M. Merz, D. Fuchs, A. Assmann, S. Uebe, H. v. Löhneysen, P. Nagel, and S. Schuppler, Spin and orbital states in single-layered $La_{2-x}Sr_xCoO_4$ studied by doping- and temperature-dependent near-edge x-ray absorption fine structure, Phys. Rev. B **84**, 014436 (2011).

[13] R. Ang, Y. P. Sun, X. Luo, C. Y. Hao, and W. H. Song, Studies of structural, magnetic, electrical and thermal properties in layered perovskite cobaltite $SrLnCoO_4$ (Lu= La, Ce, Pr, Nd, Eu, Gd and Tb), J. Phys. D: Appl. Phys. **41**, 045404 (2008).

[14] G. Subías, J. Blasco, S. Lafuerza, V. Cuartero, M. C. Sánchez, R. Boada, S. Díaz-Moreno, F. Fauth, and J. García, Relation among oxygen stoichiometry, structure, and Co valence and spin state in single-layer $La_{2-x}A_xCoO_{4\pm\delta}$ (A= Ca, Sr) perovskites, Inorg. Chem. **59**, 15757 (2020).

[15] Y. Moritomo, K. Higashi, K. Matsuda, and A. Nakamura, Spin-state transition in layered perovskite cobalt oxides: $La_{2-x}Sr_xCoO_4$ ($0.4 \leqslant x \leqslant 1.0$), Phys. Rev. B **55**, R14725 (1997).

[16] Y. Shimada, S. Miyasaka, R. Kumai, and Y. Tokura, Semiconducsemi ferromagnetic states in $La_{1-x}Sr_{1+x}CoO_4$, Phys. Rev. B **73**, 134424 (2006).

[17] H. Guo, Z. Hu, T.-W. Pi, L. H. Tjeng, and A. C. Komarek, Single crystal growth of pure Co^{3+} oxidation state material $LaSrCoO_4$, Crystals **6**, 98 (2016).

[18] A. V. Chichev, M. Dlouha, S. Vratislav, K. Knizek, J. Hejtmanek, M. Marysko, M. Veverka, Z. Jirak, N. O. Golosova, D. P. Kozlenko, and B. N. Savenko, Structural, magnetic, and transport properties of the single-layered perovskites $La_{2-x}Sr_xCoO_4$ (x=1.0-1.4), Phys. Rev. B **74**, 134414 (2006).

[19] Y. Y. Liu, X. M. Chen, and X. Q. Liu, Magnetic properties and magnetoresistance of polycrystalline $SrLaCoO_4$, Solid State Commun. **136**, 576 (2005).

[20] M. S. Andujar, D. Rinaldi, R. Caciuffo, J. Mira, J. Rivas, and M. A. S. Rodriguez, Magnetotransport properties of spin-glass-like layered compounds $La_{1-x}Sr_{1+x}CoO_4$ ($0 \leqslant x \leqslant 0.40$), Solid State Sci. **8**, 901 (2006).

[21] S. Srinath and S. N. Kaul, Static universality class for gadolinium, Phys. Rev. B **60**, 12166 (1999).

[22] N. Mott, Conduction in glasses containing transition metal ions, J. Non-Cryst. Solids **1**, 1 (1968).

[23] N. Mott, Conduction in non-crystalline materials (1993)

[24] Y. Bitla, P. Babu, and S. N. Kaul, Magnetotransport in under and optimally hole-doped bulk nanocrystalline $La_{1-x}Ca_xMnO_3$ manganites, J. Magn. Magn. Mater. **501**, 166291 (2020).

[25] M. Kriener, C. Zobel, A. Reichl, J. Baier, M. Cwik, K. Berggold, H. Kierspel, O. Zabara, A. Freimuth, and T. Lorenz, Structure, magnetization, and resistivity of $La_{1-x}M_xCoO_3$ (M= Ca, Sr, and Ba), Phys. Rev. B **69**, 094417 (2004).

[26] P. A. Joy, P. S. A. Kumar, and S. K. Date, The relationship between field-cooled and zero-field-cooled susceptibilities of some ordered magnetic systems, J. Phys.: Condens. Matter **10**, 11049 (1998).

[27] R. S. Freitas, L. Ghivelder, F. Damay, F. Dias, and L. F. Cohen, Magnetic relaxation phenomena and cluster glass properties of $La_{0.7-x}Y_xCa_{0.3}MnO_3$ manganites, Phys. Rev. B **64**, 144404 (2001).

[28] S. N. Kaul and S. Srinath, Irreversibility lines in the H-T phase diagram of re-entrant amorphous ferromagnets, J. Phys.: Condens. Matter **10**, 11067 (1998).

[29] D. A. Pejaković, J. L. Manson, J. S. Miller, and A. J. Epstein, Photoinduced Magnetism, Dynamics, and Cluster Glass Behavior of a Molecule-Based Magnet, Phys. Rev. Lett. **85**, 1994 (2000).

[30] S. Mukherjee, R. Ranganathan, P. S. Anilkumar, and P. A. Joy, Static and dynamic response of cluster glass in $La_{0.5}Sr_{0.5}CoO_3$, Phys. Rev. B **54**, 9267 (1996).

[31] J. Mydosh, Spin glasses: Redux: An updated experimental/materials survey, Rep. Prog. Phys. **78**, 052501 (2015).

[32] M. W. Haverkort, Z. Hu, J. C. Cezar, T. Burnus, H. Hartmann, M. Reuther, C. Zobel, T. Lorenz, A. Tanaka, N. B. Brookes *et al.*, Spin State Transition in $LaCoO_3$ Studied using Soft X-Ray Absorption Spectroscopy and Magnetic Circular Dichroism, Phys. Rev. Lett. **97**, 176405 (2006).

[33] S. I. Csiszar, M. W. Haverkort, Z. Hu, A. Tanaka, H. H. Hsieh, H.-J. Lin, C. T. Chen, T. Hibma, and L. H. Tjeng, Controlling Orbital Moment and Spin Orientation in CoO Layers by Strain, Phys. Rev. Lett. **95**, 187205 (2005).

[34] N. Qureshi, H. Ulbrich, Y. Sidis, A. Cousson, and M. Braden, Magnetic structure and magnon dispersion in $LaSrFeO_4$, Phys. Rev. B **87**, 054433 (2013).

[35] L. M. Helme, A. T. Boothroyd, R. Coldea, D. Prabhakaran, C. D. Frost, D. A. Keen, L. P. Regnault, P. G. Freeman, M. Enderle, and J. Kulda, Magnetic order and dynamics of the

charge-ordered antiferromagnet $La_{1.5}Sr_{0.5}CoO_4$, Phys. Rev. B **80**, 134414 (2009).

[36] Y. Bitla, S. N. Kaul, and L. Fernandez Barquín, Nonlinear susceptibilities as a probe to unambiguously distinguish between canonical and cluster spin glasses, Phys. Rev. B **86**, 094405 (2012).

[37] S. N. Kaul, Static critical phenomena in ferromagnets with quenched disorder, J. Magn. Magn. Mater. **53**, 5 (1985).

[38] N. Khan, A. Midya, K. Mydeen, P. Mandal, A. Loidl, and D. Prabhakaran, Critical behavior in single-crystalline $La_{0.67}Sr_{0.33}CoO_3$, Phys. Rev. B **82**, 064422 (2010).

[39] R. Reisser, R. Kremer, and A. Simon, 3d-XY critical behavior of the layered metal-rich halides Gd_2IFe_2, Gd_2ICo_2 and Gd_2BrFe_2, Phys. B: Condens. Matter **204**, 265 (1995).

[40] A. Arrott, Criterion for ferromagnetism from observations of magnetic isotherms, Phys. Rev. **108**, 1394 (1957).

[41] A. Arrott and J. E. Noakes, Approximate Equation of State for Nickel Near Its Critical Temperature, Phys. Rev. Lett. **19**, 786 (1967).

[42] See Supplemental Material at http://link.aps.org/supplemental/10.1103/PhysRevB.107.214405 for the modified Arrott ($M^{1/\beta}$ versus $(H/M)^{1/\gamma}$) plots for different universality classes and the isothermal magnetic entropy change ΔS_M as a function of temperature.

[43] J. Lago, S. J. Blundell, A. Eguia, M. Jansen, and T. Rojo, Three-dimensional Heisenberg spin-glass behavior in $SrFe_{0.90}Co_{0.10}O_{3.0}$, Phys. Rev. B **86**, 064412 (2012).

[44] A. Aharony and E. Pytte, Infinite Susceptibility Phase in Random Uniaxial Anisotropy Magnets, Phys. Rev. Lett. **45**, 1583 (1980).

[45] B. Dieny and B. Barbara, Random anisotropy effects on the phase transition of amorphous $Dy_xGd_{1-x}Ni$, J. Phys. France **46**, 293 (1985).

[46] E. M. Chudnovsky, W. M. Saslow, and R. A. Serota, Ordering in ferromagnets with random anisotropy, Phys. Rev. B **33**, 251 (1986).

[47] A. Ahad, K. Gautam, S. S. Majid, K. Dey, F. Rahman, R. J. Choudhary, and D. K. Shukla, Magnetic correlations in mixed valent layered $La_{1.2}Sr_{0.8}CoO_4$, Phys. B: Condens. Matter **570**, 308 (2019).

[48] S. P. Mathew and S. N. Kaul, Magnetization processes in nanocrystalline gadolinium, J. Phys.: Condens. Matter **24**, 256008 (2012).

[49] S. R. Sehlin, H. U. Anderson, and D. M. Sparlin, Semiempirical model for the electrical properties of $La_{1-x}Ca_xCoO_3$, Phys. Rev. B **52**, 11681 (1995).